EMIC triggered chorus emissions in Cluster data

B. Grison,[1] O. Santolík,[1,2] N. Cornilleau-Wehrlin,[3,4] A. Masson,[5]
M. J. Engebretson,[6] J. S. Pickett,[7] Y. Omura,[8] P. Robert,[3] and R. Nomura[9]

[1]   Electromagnetic ion cyclotron (EMIC) triggered chorus emissions have recently been a subject of several experimental, theoretical and simulation case studies, noting their similarities with whistler-mode chorus. We perform a survey of 8 years of Cluster data in order to increase the database of EMIC triggered emissions. The results of this is that EMIC triggered emissions have been unambiguously observed for only three different days. These three events are studied in detail. All cases have been observed at the plasmapause between 22 and 24 magnetic local time (MLT) and between $-15°$ and $15°$ magnetic latitude (λ_m). Triggered emissions are also observed for the first time below the local He^+ gyrofrequency (f_{He^+}). The number of events is too low to produce statistical results, nevertheless we point out a variety of common properties of those waves. The rising tones have a high level of coherence and the waves propagate away from the equatorial region. The propagation angle and degree of polarization are related to the distance from the equator, whereas the slope and the frequency extent vary from one event to the other. From the various spacecraft separations, we determine that the triggering process is a localized phenomenon in space and time. However, we are unable to determine the occurrence rates of these waves. Small frequency extent rising tones are more common than large ones. The newly reported EMIC triggered events are generally observed during periods of large AE index values and in time periods close to solar maximum.

1. Introduction

[2] Electromagnetic ion cyclotron (EMIC) waves arise from a temperature anisotropy instability [*Cornwall*, 1965; *Kennel and Petschek*, 1966]. In the plasmapause region, the ring current ion population offers a source of free energy. The density increase due to cold plasmaspheric plasma and the minimum of the DC magnetic field (**B₀**) along the field line in the vicinity of the magnetic equator maximize the wave growth in this region where these waves have been extensively studied [e.g., *Perraut*, 1982; *Roux et al.*, 1982]. However, EMIC waves have been first observed from the ground [*Harang*, 1936; *Sucksdorff*, 1936]. Because of the large variety of emission types observed from the ground, Pc1 waves [*Jacobs et al.*, 1964] were sorted by their spectral appearance [*Fukunishi et al.*, 1981] following the classification of very low frequency (VLF) emissions by *Helliwell* [1966]. The frequency-time shape of EMIC triggered emissions matches the hydromagnetic (HM) chorus spectral type. Ground based observations of HM chorus occur at a frequency below 0.5 Hz and mainly around local noon [*Fukunishi et al.*, 1981; *Anderson et al.*, 1995]. Another kind of Pc1 waves with a fine structure is the so-called "pearl pulsations" which have been studied from the ground [*Troitskaya*, 1961] and in space [*Erlandson et al.*, 1992]. In spite of the dispersive nature seen sometimes in space, pearl pulsations are not classified as HM chorus [*Mursula et al.*, 1994; *Mursula*, 2007].

[3] *Pickett et al.* [2010] recently reported the first spacecraft observations of EMIC triggered emissions in the Pc1 frequency range—an event located at the nightside plasmapause. These emissions can be classified as HM chorus. The main features of these emissions are a frequency-time dispersion, a high level of coherence, the starting frequency

[1]Department of Space Physics, Institute of Atmospheric Physics ASCR, Prague, Czech Republic.
[2]Faculty of Mathematics and Physics, Charles University, Prague, Czech Republic.
[3]LPP, Ecole Polytechnique, CNRS, Palaiseau, France.
[4]LESIA, Observatoire de Paris, Meudon, France.
[5]Science Operations Department, European Space Agency, Noordwijk, Netherlands.
[6]Department of Physics, Augsburg College, Minneapolis, Minnesota, USA.
[7]Department of Physics and Astronomy, University of Iowa, Iowa City, Iowa, USA.
[8]Research Institute for Sustainable Humanosphere, Kyoto University, Kyoto, Japan.
[9]Institut für Geophysik und extraterrestrische Physik, Technische Universität Braunschweig, Braunschweig, Germany.

Corresponding author: B. Grison, Institute of Atmospheric Physics ASCR, Prague, Czech Republic. (grison@ufa.cas.cz)

being in the range of the simultaneously observed EMIC wave emissions, and a Poynting flux propagation away from the equatorial region. Observations agree with the generation process proposed by *Omura et al.* [2010]: a phase of a linear amplitude growth followed by a nonlinear phase when the frequency increases. In addition to the EMIC seed wave, the triggering process requires a dense plasma with a population of hot protons. A mixture of plasmaspheric and ring current populations is thus adequate. Hybrid simulation—with observed values as input—reproduces the EMIC triggered emissions [*Shoji and Omura*, 2011]. These triggered waves strongly modify the velocity distribution function of the hot proton component, and part of the scattered protons can precipitate into the ionosphere. When both the energetic proton density and the temperature anisotropy are high enough, successive triggered emissions are observed in simulation results [*Shoji et al.*, 2011]. Moreover, proton scattering by these multiple triggered emissions results in EMIC wave generation below the local He^+ gyrofrequency (f_{He^+}). More recently, thanks to new simulations, *Shoji and Omura* [2012] report the possibility of triggering EMIC waves on the He^+ branch. These emissions required a hot proton population with a higher energy than the one required along the proton branch. All these results are based on the single event (30 March 2002) of EMIC triggered chorus emissions reported by *Pickett et al.* [2010].

[4] The Cluster [*Escoubet et al.*, 1997] data survey performed for this paper aims to increase the number of documented events in order to improve our understanding of these emissions. After the methodology description, we detail three new cases of EMIC triggered emissions. The properties of these emissions are investigated through polarization and Poynting flux studies. In the discussion, we comment on the accuracy of our methodology with regard to the results, the location of the observations, and the general properties of the triggered emissions.

2. Methodology

[5] Onboard Cluster, the [1.5–2.7] Hz range of the triggered emissions observed by *Pickett et al.* [2010] is accessible through the FGM and STAFF-SC instruments, which have a similar sampling frequency in the normal mode (22.5 and 25 Hz, respectively). The sensitivity curves of the two instruments intersect close to 1 Hz, FGM sensitivity being better below this frequency and STAFF-SC better above it [*Nykyri et al.*, 2006]. In order to maximize our chance to detect weak emissions in that frequency range, we carried out a STAFF-SC data survey. The STAFF instrument [*Cornilleau-Wehrlin et al.*, 2003] measures magnetic fluctuations from 0.1 to 4 kHz. Waveform data at the output of a low pass filter are obtained up to 12.5 Hz in the normal mode and up to 225 Hz in the high bit rate mode. The lower frequency limit for three component studies is 0.35 Hz in a non-spinning coordinate system (CS) due to the spin frequency. In the fixed SR2 (Spin Reference) coordinate system, the waveform along the spin axis component is valid from 0.1 Hz.

[6] A quicklook database available at the Cluster Active Archive (CAA, http://caa.estec.esa.int) collects 3-hour plots of STAFF-SC data. Each plot displays the power spectral density (PSD) of the magnetic field fluctuations versus time

and frequency (spectrogram) of the component parallel to the spin axis, for the four spacecrafts. The triggered emissions have been observed at frequencies close to one half of the local proton gyrofrequency (f_{H^+}). $f_{H^+}/2$ is within the [0.1–12.5] Hz range for $\mathbf{B_0}$ values within a [14–1660] nT range. Along the Cluster orbit, $\mathbf{B_0}$ is usually within this range, except for parts of the magnetotail and in the solar wind region where it might be lower and, since 2007, close to perigee where it is higher. Using the STAFF-SC database, we do not make any assumptions about the places where new cases of EMIC triggered emissions can be observed in the magnetosphere, and the STAFF-SC instrument frequency range matches the HM chorus frequency range based on ground observations [*Fukunishi et al.*, 1981].

[7] A visual inspection of these preexisting plots of the STAFF-SC instrument data was carried out over the years 2000–2008. This led to a downselected list of about 20 candidates of EMIC triggered emissions based on the observation of a possible frequency with time dispersion. Special attention was paid to the inner magnetosphere region. After this downselection, polarization, coherence and Poynting vector analysis was performed for each date in this list to pick out new cases of EMIC triggered emissions. Finally, we unambiguously found triggered emissions for only three more Cluster orbits. In the discussion section, we address the influence of our methodology on this small number of events.

3. Observations

[8] For the three time intervals we identified with EMIC triggered emissions, we first look at the characterization of the magnetospheric region. Then, we compare the observations on the four spacecrafts, before analyzing in depth the most intense triggered emissions.

3.1. First Event: 26–27 March 2003
3.1.1. Overview of the Ultra Low Frequency (ULF) Emissions

[9] On 27 March 2003, around 0000 universal time (UT, hereafter time value without units are expressed in UT), the Cluster fleet crossed the magnetic equator when approaching its perigee. Figure 1 presents (a) spacecraft potentials, (b) spacecraft 4 (SC4) proton energy flux dynamic spectrum and (c) four magnetic PSD spectrograms. Spacecraft potential is known to be a good qualitative indicator of the surrounding plasma density: the higher the potential, the more dense the plasma. It can also be used for precise plasma density measurements [*Masson et al.*, 2009; *Moullard et al.*, 2002]. When the surrounding plasma is dense enough to compensate for all the photoelectron losses (for Cluster around 100 cm^{-3}), the spacecraft potential saturates, approaching 0 V, and the density can no longer be derived from it. In the present case, the potential of each spacecraft reaches a plateau during at least 30 min. This region of denser plasma is encountered successively by spacecrafts 1, 2, 4 and 3. The potential maximum is the highest for SC4 and SC2 and a bit lower for SC1. SC3 potential displays the lowest maximum. This spacecraft order (4,2,1,3) also sorts the time duration of the plateau in a decreasing order.
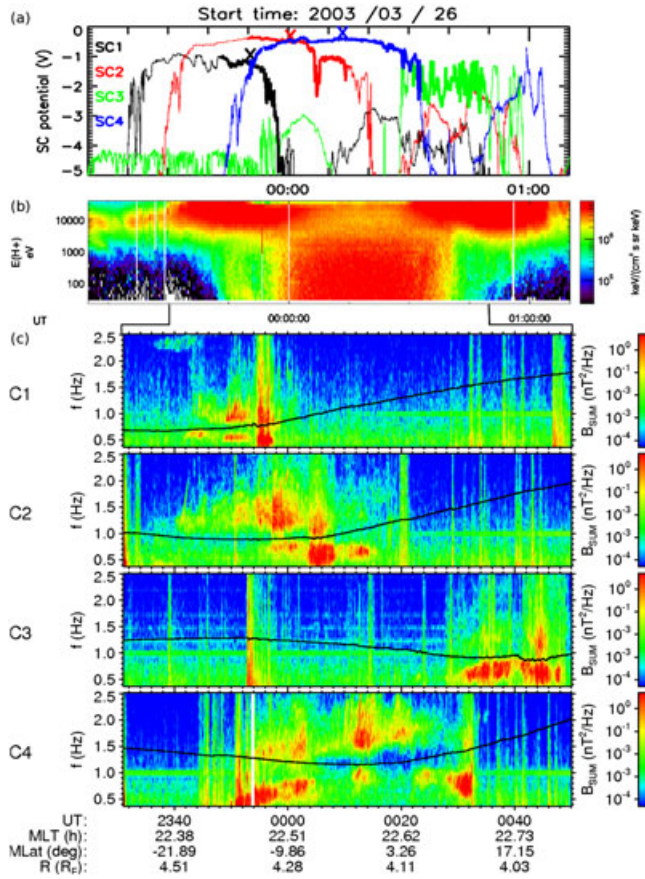
Figure 1. Top panel (a): Spacecraft potential in volts (EFW data) of the Cluster fleet versus UT (color code is indicated on the plot left side). Middle panel (b): Proton energy flux versus time and energy range (SC4, CODIF data). Lower panels (c): Total magnetic power spectral density (PSD) (STAFF-SC data) versus time and frequency for each spacecraft. f_{He^+} is overplotted in black. The position of SC4 is indicated for each time mark.

[10] CIS/CODIF instrument data of SC4 (Figure 1b) show the presence of a ring current population (energetic protons above 10 keV) on each side of the potential plateau. When the spacecraft potential reaches its maximum, the most energetic part of a cold ion population is detected. Taking into account the 4.2 R_E radial distance of the spacecraft from the Earth (cf. position indication for each time mark of Figure 1c), we identify this cold population as a plasmaspheric population. Consequently, the strong potential gradient delimits the plasmapause entry and the high potential region corresponds to the edge of the plasmapause. The plasmasphere population energy flux detected by SC4 is the most intense (followed in a decreasing intensity order by SC3 and SC1, not shown). SC2 and SC4 are going the deepest into the plasmapause while SC1 and SC3 are only skimming it.

[11] The four bottom panels of Figure 1c display ULF magnetic wave activity recorded by the STAFF-SC instrument on-board each spacecraft between 0.35 and 2.5 Hz. For the sake of clarity, we focus on the time and frequency ranges that contain all the intense wave emissions recorded during the given time interval. On the spacecraft potential

panel, lines are drawn in bold when persistent intense magnetic fluctuations (larger than 0.1 $nT^2 Hz^{-1}$, excluding bursts of activity) are detected. The wave activity appears to be clearly linked to the plasmapause entry. EMIC activity has been observed in this region for a long time [*Bossen et al.*, 1976; *Labelle et al.*, 1988, eg]. Moreover, intense waves are not detected outside of the plasmapause. With the exception of a wave burst seen on SC2 at 2335, SC1 and SC2 record the most intense wave activity on the exit of the plasmapause boundary layer. SC4 detects waves over almost the whole plasmapause crossing and SC3 mainly at the plasmapause entry. Strong magnetic wave activity is recorded continuously at the edge of the plasmapause during more than 1 h between 2340 and 0048. EMIC waves are detected below and above f_{He^+} (black line plotted over each spectrogram). The lack of waves in the vicinity of f_{He^+} is well documented from GEOS [*Young et al.*, 1981] or ATS [*Mauk et al.*, 1981] observations: waves are absorbed through the cyclotron resonance with cold He^+ ions. SC1 detects the same level of wave activity below and above f_{He^+}. At SC2 and SC4, the wave intensity level is higher below f_{He^+} at the plasmapause entry, while it is higher above f_{He^+} deeper in the plasmapause. Waves are significantly more intense below f_{He^+} at SC3.

[12] As indicated by the position of SC4 for each time mark, the spacecraft is close to the magnetic equator when detecting the emissions: the magnetic equatorial plane is roughly crossed in the middle of the plateau of the potential, which corresponds to a [−15°, +15°] magnetic latitude (λ_m) interval. This is also true for the other satellites. The location of these emissions can thus be considered as typical for EMIC waves: the density gradient and the minimum of $\mathbf{B_0}$ along the field line maximize the wave destabilization through temperature anisotropy of the energetic ion population from the ring current. The lack of intense waves at SC1 and SC2 entries suggest that the plasma conditions allow intense wave destabilization only after 2340. As a confirmation, the ion temperature anisotropy measured by the CIS instrument onboard SC1 is higher after 2340 than before (not shown).
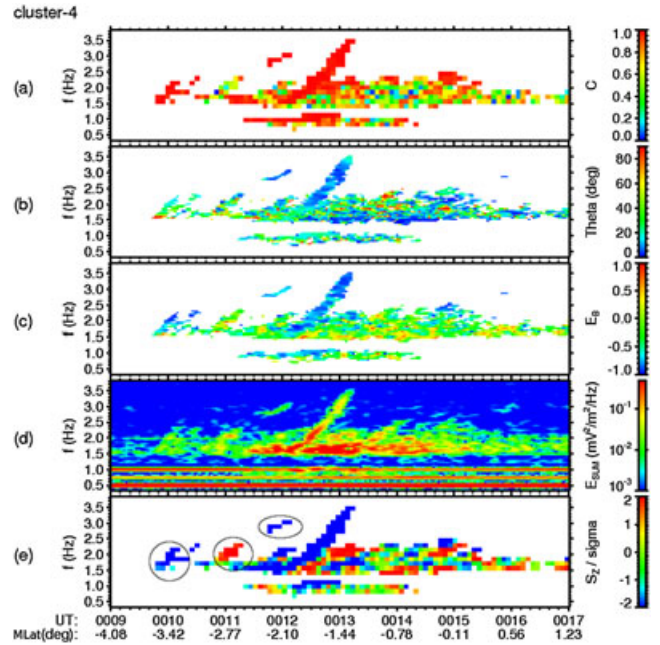
3.1.2. Triggered Emissions

[13] Figure 2 presents a focus on time intervals when dispersive magnetic emissions are observed. On SC1 (Figure 2a) a succession of rising tones (at least three) are seen between 2348 and 2352. The increase of the frequency is rather small: from 0.9 Hz to 1.25 Hz for the largest one. On SC2 (panel 2b) the rising tone—at 2341—displays a comparatively lower PSD, but a larger frequency extent, from 1.1 to 2 Hz for a slope of 90 s Hz^{-1} (following the unit used in *Pickett et al.* [2010]). At 0012 on SC4 (Figure 2c), the rising tone is the most intense, and its frequency increase is the largest. The tone starts at about 1.7 Hz and disappears around 3.5 Hz for a total duration of about 45 s. The corresponding slope is about 26 s Hz^{-1}. At the same time, a lower frequency dispersive structure seems to occur below f_{He^+} (cf. also figure 1). Smaller and weaker rising tones are seen before and after 0012.

[14] A detailed analysis of polarization and propagation properties of the event recorded on SC4 is given in
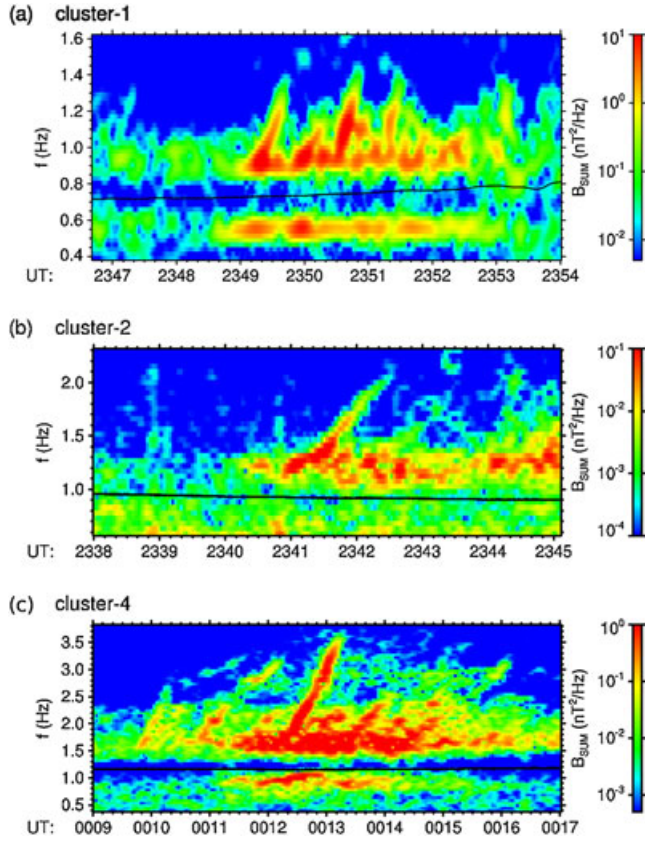
Figure 2. Focus on the time intervals when rising tones are observed. Total magnetic PSD spectrogram (STAFF data) for (a) SC1, (b) SC2 and (c) SC4.

Figure 3. Detailed analysis of the electromagnetic properties of the waves at SC4: (a) coherence level, (b) propagation angle θ, (c) ellipticity, (d) total electric PSD and (e) the sense of propagation of the Poynting flux parallel component. Only the spectrogram parts with a total magnetic PSD value larger than 0.05 nT^2 Hz^{-1} are plotted on Figures 3a, 3b, 3c and 3e. Coherence and Poynting sign panel resolution is lower because their computation requires averaging and normalizing neighboring values.

Figure 3. The polarization properties (Figures 3a, 3b and 3c) are computed through the singular value decomposition (SVD) analysis method [*Santolík et al.*, 2003]. Electric PSD (Figure 3d) is used in addition to the magnetic PSD to estimate the direction of the parallel component of the Poynting flux (Figure 3e) via the method presented in *Santolík et al.* [2001]. We first detail the properties of the previously mentioned large rising tone. Its level of coherence (Figure 3a) is particularly high compared to the level of the EMIC waves. High coherence values indicate that the cross-power spectrum average is low in the polarization plane and hence a constant phase between magnetic components and a strong level of polarization [*Santolík and Gurnett*, 2002; *Santolík et al.*, 2002]. The wave vector is almost aligned with $\mathbf{B_0}$ (low values in Figure 3b). The riser polarization is left-handed and circular (ellipticity values close to –1 in Figure 3c). The electromagnetic nature of that emission is highlighted by the electric counterpart seen on Figure 3d. The rising tone clearly propagates in a direction anti aligned with $\mathbf{B_0}$ as is indicated by the negative values on Figure 3e. Assuming a dipolar magnetic field, the magnetic latitude of the spacecraft is negative at that time: the electromagnetic riser propagates away from the magnetic equatorial region. The properties of the tone are similar to those reported by *Pickett et al.* [2010]; *Omura et al.* [2010] for the rising tones, which they classified as EMIC triggered emissions. In addition, spacecrafts are located in both cases at the edge of the plasmapause nightside in the presence of a hot proton population. We can thus unambiguously identify this rising tone as an EMIC triggered emission.

[15] It is difficult to perform an analysis of the same quality for the other rising tones because of their weaker intensity and of their smaller frequency extent. Focusing on the time period before 0012, three dispersive electromagnetic structures (delimited by black solid lines) are observed in Figure 3e. Two of them are anti-aligned with $\mathbf{B_0}$, at 0010 and at 0012—below and above 2 Hz. A single dispersive emission is field aligned—at 0011. It is worth to notice that waves propagating away from the equatorial plane direction (λ_m is negative) also display the highest level of coherence (Figure 3a). *Omura et al.* [2010] have shown that the conditions for rising tone generation maximize at the magnetic equator and that the resulting emission is highly coherent. We therefore classify as triggered emissions only the two dispersive and highly coherent emissions propagating away from the equatorial plane. The presence of a triggered emission above 2 Hz, far from the main band EMIC waves, is unexpected. The lower part of the rising tone could interact with the non-coherent waves seen at 0011 where it might be hidden. This also occurs just before 0000 on SC2 (cf. Figure 1). The coherence level appears as the most relevant criterion to differentiate between triggered emissions and EMIC wave packets occurring by chance in a seemingly dispersive structure. The rising tones observed at SC1 display a high level of coherence. The tone with a large frequency extent at SC2 is too weak to be properly analyzed.

Table 1. Spacecraft Crossing Time and Location at the Magnetic Equator

SC	Time (UT)	MLT (h)	D (R_E)
1	2340	22.6	4.80
2	2355	22.4	4.50
4	0015	22.6	4.15
3	0040	22.5	4.35

Triggered emissions with a small frequency extent appear to be more common than the ones with a large frequency extent. Hereafter, "small" and "large" (rising tones) refer to their frequency extent while "weak" and "intense" refer to their power.

[16] The absence of risers at SC3 might result from a lack of seed waves as wave intensity above f_{He^+} is weak. One could ask why the waves are located preferentially below f_{He^+} at SC3. At SC2 and SC4, the waves are more intense below f_{He^+} at the edge of the plasmapause and above f_{He^+} deeper in. SC3 encounters only the region of intense emissions below f_{He^+}. *Roux et al.* [1982] noticed that EMIC waves above f_{He^+} were more sensitive to the He^+ concentration than below f_{He^+}. Due to the ionospheric origin of the He^+ population one expects a higher He^+ concentration inside the plasmasphere than at its edge. This then confirms that SC3 is just skimming the plasmapause as already noticed on Figure 1. Considering Table 1, all spacecrafts cross the equatorial plane at a similar MLT. SC3 is at an intermediate distance from Earth (SC4 is the closest and SC1 the most distant). Nevertheless SC3 is not penetrating as deep into the plasmasphere as SC1 and SC2 even though its position is closer to the Earth. A plausible explanation (also supported by WHISPER data—not shown) is a move of the boundary toward Earth between 2355 and 0040.

[17] In relation to the case reported by *Pickett et al.* [2010], observations differ here from one spacecraft to another. The intercraft separations are much larger for this event—from 5000 km to 18500 km—compared to 250 km for the Pickett case. The present case illustrates that the triggering process is a localized phenomenon in space and time.

3.2. Second Event: 8 March 2004

3.2.1. Multi Spacecraft Observations

[18] On 8 March 2004 at 0830 UT, the Cluster fleet approached the magnetic equator from the southern hemisphere in the following order: spacecrafts 1, 3, 2 and 4. At that time, the minimum and maximum separation distances, respectively, were 240 and 1090 km. Showing results of the same analysis as for the previous event, Figure 4 presents the spacecraft potentials (top panel) and the total magnetic PSD (bottom panels). The potential increase seen on each spacecraft is interpreted as the entry to the plasmasphere following the previously mentioned order. As is seen on the bottom panels, each spacecraft encounters a wave activity enhancement just above f_{He^+} (black line) during a time interval of 3 min—still in the same spacecraft order. The center time of these emissions is reported on the panel of the SC potential (colored circles). The wave activity location is just
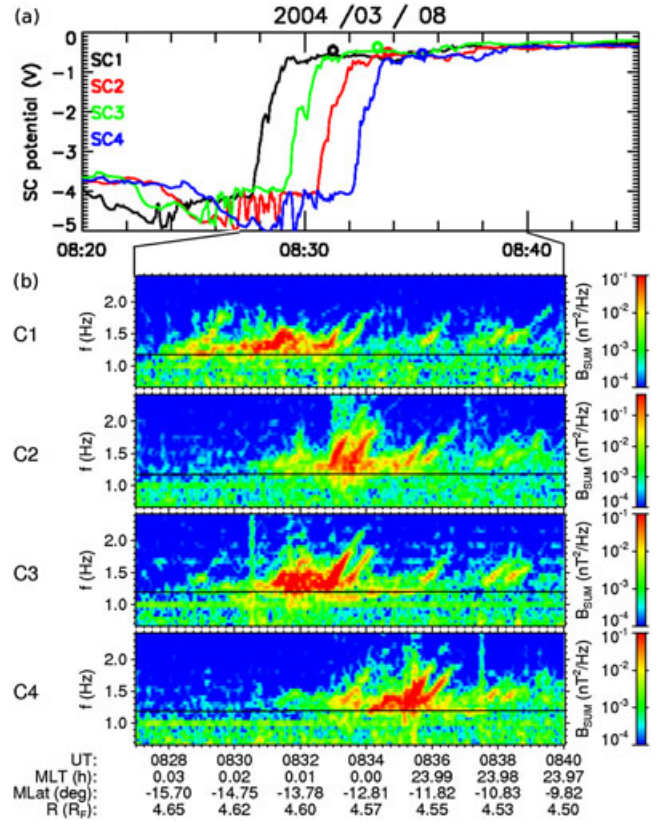
Figure 4. (a) Spacecraft potentials and (b) total magnetic PSD for the four Cluster spacecrafts. Circles on potential plots indicate the time of most intense triggered emissions.

inside the plasmapause density gradient. Once again, it is a typical location for EMIC emissions destabilized by the gradient density of the plasmapause. The emissions process occurs continuously at least between 0830 and 0836. The spectral power maximum ($\approx 10^{-1}$ nT^2 Hz^{-1}) is weaker by almost two orders of magnitude than the one detected in the previous event.

[19] Considering the magnetic wave activity, SC 2, 3 and 4 detect two dispersive structures that can be considered a priori as EMIC triggered emissions (as shown hereafter). On all spacecrafts smaller and less intense rising tones are observed outside of the main wave activity region. We focus now on the largest ones. The foot of these emissions is embedded in the EMIC waves at about 1.3 Hz, just above the local f_{He^+} (plain black line). The highest frequency of the risers is between 1.9 and 2 Hz. The duration of triggered emissions is about 60s leading to a slope of 77 s Hz^{-1}. The most intense risers are detected on SC2, but they display a curvature that is observed neither on SC3 nor on SC4. The curvature can be due to a change of group velocity or it can result from a perturbation during the propagation.

[20] The SC2 and SC3 detect the two rising tones at almost the same time. It is not clear whether both spacecrafts observe the same riser. On the one hand, the spacecraft separation (240 km) is close to one reported by *Pickett et al.* [2010] when all four spacecrafts detected similar risers. On the other hand, the frequency-time shape looks different. The separation is mainly transverse to $\mathbf{B_0}$ (238 km versus 31

Table 2. Spacecraft Location at Times of Intense EMIC Emissions for SC1 and Rising Tones for Other Spacecraft

SC	Time (UT)	MLT (h)	λ_m (°)	D (R_E)
1	0831	0.012	−13.1	4.60
2	0833	0.007	-13.4	4.61
3	0833	0.004	−13.1	4.58
4	0835	0.015	−13.2	4.59

km along $\mathbf{B_0}$). As the risers propagate along $\mathbf{B_0}$, the spacecraft separation supports the possibility that spacecrafts 2 and 3 detect different risers assuming that a source region size is less than 240 km.

[21] As SC4 follows SC3 with a 2 min shift in latitude and geocentric distance and with a small separation in MLT (cf. Table 2), one can consider that the two intense rising tones seen on SC4 are not the same as the ones detected on SC3. However, the triggering process is still active when SC4 is crossing the EMIC region. Based on the *Pickett et al.* [2010] observations, the recent simulation results from *Shoji and Omura* [2011] showed that the triggering process occurs in a repetitive way as long as energetic protons are present. We believe that the four consecutive risers observed on three spacecrafts nicely illustrate this result. However, there is no evidence of EMIC emissions below f_{He^+} in the present case.

[22] Two alternatives can explain the lack of intense rising tones at SC1: (1) a spatial effect, i.e., SC1 can be on the edge of the triggered emissions region or (2) a temporal effect i.e. the triggering emission process is not active yet when SC1 is entering the plasmapause. SC2 follows SC1 in latitude and geocentric distance by about 2 min (cf. Table 2). The MLT of SC1 is intermediate between those of SC2 and SC4. Consequently, absence of risers at SC1 is best explained by the fact that the triggering emission process had not started yet when SC1 was crossing the region.

3.2.2. Single Spacecraft Observations

[23] Emission properties of the SC3 data are presented in Figure 5. As noticed previously, the most intense emissions are detected between 0830 and 0835 when the spacecraft was located close to midnight MLT, at a magnetic latitude of −15° at a distance of about 4.6 R_E from the Earth. The coherence level (Figure 5a) is larger for the first rising tone than for the second one and than for the EMIC background emissions. The propagation angle (Figure 5b) of the first rising tone displays also larger values (close to 90°) than for the other emissions. From Figure 5c, the low frequency part of the EMIC waves has a circular sense of polarization, namely right-handed. Rising tone polarization is close to linear (ellipticity close to 0). The polarization properties of the emissions are confirmed by the analysis of the data from the three other spacecrafts (not shown). The first rising tone is also the only feature clearly coming out from the electric field data (Figure 5d). Harmonics of the 0.25 Hz spacecraft spin frequency are more intense than the other emissions. Nevertheless, the Poynting vector (Figure 5e) is clearly anti-field aligned (blue color), which means that the first rising tone is propagating away from the magnetic equatorial plane region.

[24] The properties of the first rising tone—its sense of propagation, its high coherence value and its electromag-

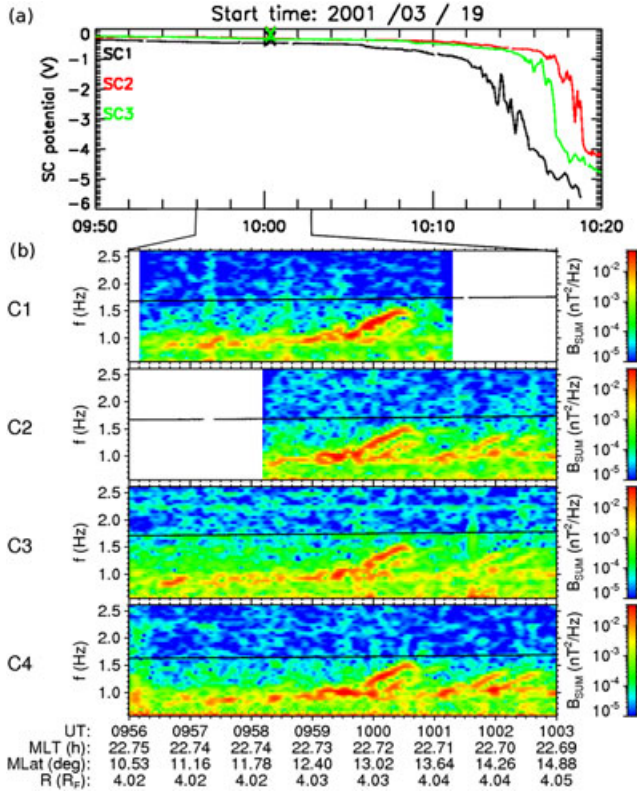cluster-3 : 2004-03-08 08:27:00.105 - 2004-03-08 08:40:00.905
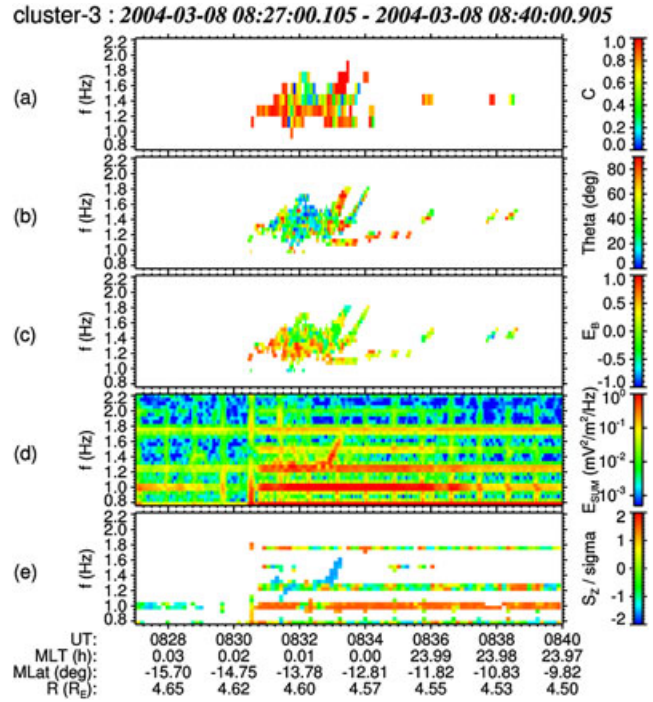
Figure 5. Electromagnetic properties of the waves at SC3. Cf. Figure 3 for the panel details.

netic nature—in addition with the frequency-time dispersion are solid arguments to identify it as a triggered EMIC emission. For the previously described triggered emissions, in this paper and by *Pickett et al.* [2010], the wave vector is almost aligned with $\mathbf{B_0}$ and the polarization is left-handed. In the present case, observations take place much farther from the generation site located close to the equatorial plane. An increase of the angle during the propagation is thus a plausible explanation of the observed large values of $\theta_{k,B}$. This propagation effect has already been observed for EMIC waves in a rich He^+ plasma [*Young et al.*, 1981]. A larger angle explains also the linear polarization aspect. The second rising tone appears narrower and weaker than the first one. Because calculation of the coherence parameter requires averaging values over consecutive time and frequency intervals, this averaging process will include also values, which are not part of the narrow rising tone. Consequently, the coherence level is artificially decreased. Despite its low coherence value, we consider the second riser as a triggered EMIC emission as well. For the same reason, it is not possible to properly analyze the numerous small and weak rising tones seen later.

3.3. Third Event: 19 March 2001
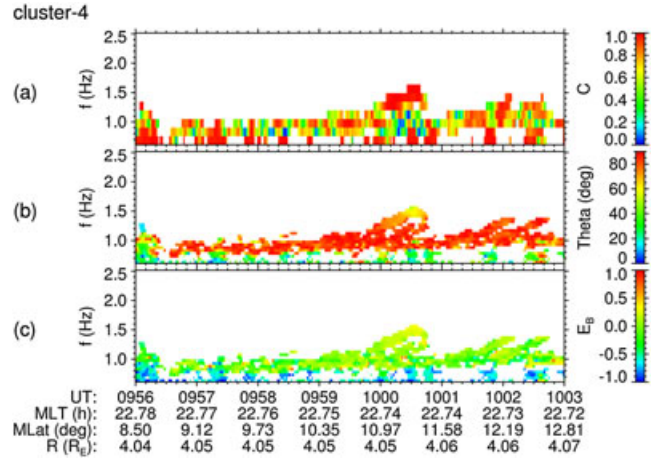
3.3.1. Multi Spacecraft Observations

[25] Figure 6 presents the spacecraft potentials and the total magnetic PSD for the event observed on 19 March 2001. As shown in the top panel, spacecrafts 1, 3 and 2 exit the plasmapause in this order starting from 1010. The EMIC wave activity intensity detected close to 1 Hz on all spacecraft is rather low: the maximum magnetic PSD is about 0.01 nT^2 Hz^{-1}, which is lower by an order of magnitude compared to the second case (and by three orders

Figure 6. (a) Spacecraft potentials and (b) total magnetic PSD for the four Cluster spacecrafts (no potential data available for SC4). Crosses on potential plots indicate the time of the most intense triggered emissions.

Figure 7. Electromagnetic properties of the waves at SC4. Cf. Figure 3 for the panel details.
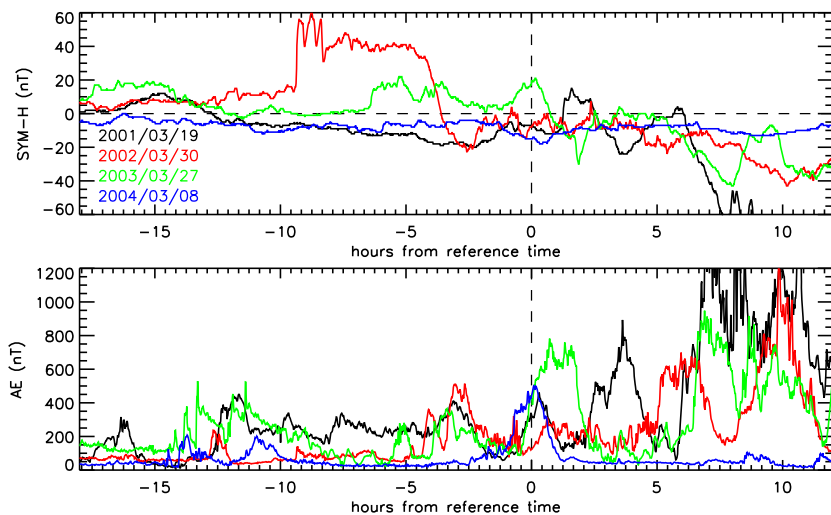
3.3.2. Single Spacecraft Observations

[27] We present in Figure 7 the polarization properties at SC4—where the most intense rising tones are observed—obtained through the same methods as for the two previous events. As mentioned previously, the coherence estimation for such short emissions is a challenge. Nevertheless, the coherence value (Figure 7a) of the largest dispersive tone is clearly higher than the classical EMIC waves at 1 Hz. The wave propagation angle (Figure 7b) is oblique (red color of the theta values) and the polarization (Figure 7c) is close to linear, but slightly right-handed (green to yellow color). These properties are confirmed by other spacecraft data (not shown). The Poynting analysis could be achieved only for two spacecrafts (2 and 3) and leads to inconclusive results (not shown). The weakness of the emissions and the spin frequency harmonics in the electric field data can explain the difficulty to obtain conclusive results.

[28] Nevertheless, we believe these rising tones to be triggered emissions because of the clear frequency-time dispersion of the emissions and the highly coherent structure of the tones. The observations of the large rising tone by the four spacecrafts is also supportive of this assertion. Simulation results of triggering emissions along the He^+ branch [*Shoji and Omura*, 2012] support the observations of EMIC triggered emission below f_{He^+}. Propagation effects explain the polarization change from the place of generation [*Young et al.*, 1981].

3.4. SYM-H and AE indices

[29] *Pickett et al.* [2010] noticed that prior to their observations, the SYM-H index was above 20 nT for several hours, indicative of a strong compression of the magnetosphere and of a possible magnetic substorm. Figure 8 gathers SYM-H [*Iyemori et al.*, 1999; *Sugiura and Poros*, 1971] and AE [*Davis and Sugiura*, 1966] indices during the four events (including the one published in *Pickett et al.* [2010]). SYM-H takes positive values when the magnetosphere is compressed and the AE index rises with auroral activity intensification. AE is a good indicator of energetic particle precipitation in the auroral zones. The reference

of magnitude compared to the first one). The most striking feature is the rising frequency emissions seen between 1000 and 1002. The largest frequency extent—detected on the four spacecrafts—is from 1.1 to 1.4 Hz. The corresponding slope is about 80 s Hz^{-1}. The spacecraft potential is still saturated at this time: observations are obviously made deeper in the plasmasphere than previously. As the density gradient of the plasmapause and the minimum of $\mathbf{B_0}$ at the magnetic equator are known to be more favorable for destabilization of EMIC waves, the location can explain the weakness of the emissions because of an attenuation during the propagation from the equatorial region. The solid black line represents the local He^+ gyrofrequency. For the first time in our observations, the rising emissions are observed below f_{He^+}.

[26] Compared to the previous cases, the observations take place closer to the Earth ($4\,R_E$), at a high magnetic latitude (above $10°$) and in the night sector (about 00MLT). The closest and largest intercraft separations are 520 and 1610 km, respectively. It is an intermediate configuration with respect to the preceding cases. The separations between satellites projected in the plane perpendicular to $\mathbf{B_0}$ vary from 230 to 940 km. Compared to the second event where SC2 and SC3 observe different frequency-time shapes at a perpendicular separation of only 240 km, the rising tones here look the same at each spacecraft, which might be indicative of a larger source region or of a less dispersive propagation.

Figure 8. Time evolution of SYM-H (top panel) and AE (bottom panel) ground magnetic indices for the four reported cases of EMIC triggered emissions in the Cluster data (the line color indicates the event per the color code for each date indicated in the top panel). Abscissa is given in hours with respect to the detection time of these emissions. The reference time of each event is 1000, 0800, 0000 and 0830 (UT), respectively.

time (RT) is the detection time of triggered emissions. Index evolutions during each event are plotted from RT–18h to RT+12h. Prior to the reference time, positive SYM-H values are observed for the 2002 event (60 nT), the 2003 event (20 nT) and the 2001 event (10 nT). The positive period lasts less than 5 h for the 2001 event. The SYM-H index of the 2004 event maximizes at RT–17 h (0 nT) and minimizes close to RT (–15 nT). Large risers are detected in 2002 and 2003 when the magnetosphere is highly compressed before the observations.

[30] The AE index (bottom panel) is usually large (> 300 nT) around the RT. However, it has much larger values later on (5–10 h) for three dates. A really quiet evolution is observed for the 2004 event, but the triggered emissions were observed precisely at the single peak larger than 200 nT. For this event, with no magnetosphere compression, we believe the spacecrafts were at the right time at the right place to detect triggered emissions. The three other events are observed during periods of enhanced auroral activity. The disturbed overall geomagnetic conditions, reflected by large AE values, cause the onset of EMIC waves [*Clausen et al.*, 2011] and mixing of cold and hot populations close to the plasmapause. This explains the observed coincidence of high AE and triggered emissions even if there is no causal link. This link between the triggered emission occurrence and the solar activity appears also in the date of the events. There is one event per year between 2001—a few months after the beginning of the Cluster science operations—and 2004 and none after when Cluster was still crossing the plasmapause region. Therefore, there was nothing preferential in the Cluster orbit that made it more likely to observe these events near solar maximum. We thus conclude that EMIC triggered emissions are generally observed at the plasmapause nightside during a period of large solar activity (the last maximum of the 11 years cycle of solar activity was reached in 2001).

4. Discussion

4.1. Low Number of Events

[31] The three cases of EMIC triggered emissions presented here demonstrate that the observation reported by *Pickett et al.* [2010] is not a unique case. However, this low number of events identified over eight years of Cluster data is questionable: are these emissions so unusual or is our method too restrictive? We briefly recapitulate the arguments presented in Section 2 in favor of the method: possibility of a survey of magnetic spectrograms during the whole duration of the Cluster mission without any assumption on the location of the EMIC triggered emissions.

[32] The 3 h plot duration does not seem to affect the detection as short duration events are detected. The frequency scale (0.1 – 12.5 Hz) makes difficult the visual detection when the emissions hit only the lowest part of the spectrum. Actually, two of the three cases are observed below 1 Hz with a short dispersion in frequency. So, here we consider that we could have missed lower frequency cases. In the three reported events, numerous weak and small dispersive tones are observed before and after the large—and visually detected—rising tones. Reporting cases with only such weak and small rising tones requires a specific study. The component plotted on each spectrogram is roughly anti-aligned with the *z* axis of the GSE coordinate system, except during special measurement campaigns as for SC3 in May 2008. In the equatorial region, this component mainly measures fluctuations parallel to the background magnetic field. Regarding the first reported case, it might not be the best component as the fluctuations are mainly lying in the perpendicular plane, but the fluctuations along the *z*-axis were intense enough to be easily identified. However, the EMIC triggered emissions of the 2001 event are clearly seen on the *z* component when they are hardly observed on the two other components. So, considering only one component, the

z-axis seems to achieve the best results: we identify a new case with mainly perpendicular fluctuations and we could also identify cases with parallel fluctuations that are not seen in the perpendicular plane. The triggered emissions result from a purely transverse generation [*Omura et al.*, 2010] mechanism. Thus, considering the z component, we identify all kinds of events: emissions are the most intense at their generation when even a small fraction can be identified along z.

[33] All triggered emissions are detected in the equatorial region. The highly polar orbit of Cluster certainly limits the number of newly identified events. The triggered emissions are not detected at high latitudes along the Cluster orbit. The detection of EMIC triggered emissions below f_{He^+} changes the perspective of the survey. In the instrument frequency range [0.1–12.5] Hz, the minimal and maximal $\mathbf{B_0}$ values corresponding to half of f_{He^+} are 53 and 6670 nT, respectively. This means that He^+ EMIC triggered emissions cannot be detected in the distant magnetosphere. In the innermost part, the instrument saturates as Cluster perigee has become much closer to the Earth than initially foreseen. This can explain why only one case of this emission has been identified.

[34] Our method allowed us to identify new cases with various polarization properties. However, it is not adapted to detect the numerous weak and/or short triggered emissions and the low frequency rising tones, specially below f_{He^+}. Therefore, we are unable to determine the occurrence rates of these emissions.

4.2. Properties

[35] The main characteristic of the triggered emissions is their frequency-time dispersion. They extend above the frequency of the EMIC wave packet they emerge from (above or below f_{He^+}). Coherence values are clearly higher for the rising tones than for the EMIC waves. These two criteria allow us to identify triggered emissions unambiguously. In addition to the three cases presented here, we consider also the event presented in *Pickett et al.* [2010] to discuss the EMIC triggered emission properties based on Cluster observations. Properties are gathered in Table 3. For each date (column *a*) we present the region extension (*b-d*) where the rising tones are observed. In the next columns, we focus on the Poynting flux orientation (*e*), on the wave PSD (*f*), on the time-frequency dispersion (*h-j*) and on the polarization (*k-m*) of the most intense tone for each event.

[36] All the recorded triggered emissions are located close to the plasmapause nightside (between 22 and 24 MLT, [4.0; 4.8] R_E) and close to the equatorial plane ($|\lambda_m| < 15°$). This result is not surprising as the plasmapause is one of the preferred regions for EMIC waves that are the seed emissions for the triggering process. On the other hand, *Anderson et al.* [1992]; *Fraser* [1982]; *Usanova et al.* [2012] have statistically shown—in the equatorial plane—a larger occurrence of EMIC waves at larger L values on the dayside of the magnetosphere. The lack of observations by Cluster in that region can be explained by an orbital effect: the highly polar and eccentric Cluster orbit limits observations in the equatorial plane of the dayside magnetosphere. The triggered emissions require not only EMIC waves, but also a hot proton component. This component is more frequently observed close to the plasmapause (ring current, injections of a hot population after magnetic substorms) than in the outer dayside region. A less dense hot population implies a lower frequency extent of the triggered waves, which makes the detection of triggered emission more challenging in this region. The extension of the plasmasphere is larger on the duskside. As the triggered emissions are observed close to the perigee, we consider the Cluster orbit can affect the detectability of the triggered emissions on the duskside/afternoon side of the plasmapause.

[37] For two additional cases, we could demonstrate that the parallel component of the Poynting vector is directed away from the equatorial region. This property is consistent with the theory of EMIC triggered emission generation via proton phase space holes as developed by *Omura et al.* [2010]. Other properties of triggered emissions seem to be latitude dependent: close to the magnetic equator (30*March*2002 and 26*March*2003 events) the PSD value is large, the frequency extent is large, the frequency sweep rate is high, the polarization is fully circular (left-hand) and the wave vector lies along the magnetic field line (cf. Table 3). Conversely, farther from the equator (19*March*2001 and 08*March*2004 events) the PSD is weaker, the frequency extent is smaller, the sweep rate is lower, the polarization is more linear (with some RH aspects) and the propagation is oblique. As previously mentioned, the change in polarization can be explained by propagation effects. These effects also affect the group velocity, and it probably explains the difference observed in the frequency sweep rate. The rising tones with short frequency extent are more numerous than the events with a large frequency extent but

Table 3. Comparison of the Four Reported Events[a]

(a) Event	(b) MLT (h)	(c) $\lambda_m(°)$	(d) D (R_E)	(e) $\vec{\Pi}$	(f) PSD	(g) f_{He^+}	(h) f_0	(i) f_m	(j) df/dt	(k) Polar.	(l) Sense	(m) $\theta_{(k,B)}$
19 March 2001	[22.7;22.7]	[10.9;14.4]	[4.0;4.1]	?	< 0.1	1.7	1.0	1.5	$9.6e^{-3}$	Lin	RH	> 60°
20 March 2002	[22.2; 22.4]	[−4.0; +6]	[4.4; 4.5]	A	> 100	0.9	1.6	3.1	$3.4e^{-2}$	Circ	LH	< 20°
26 March 2003	[22.3; 22.6]	[−9.0; +3]	[4.1; 4.8]	A	> 100	1.1	1.6	3.5	$3.2e^{-2}$	Circ	LH	< 20°
08 March 2004	[0.0; 0.01]	[−13; −14]	[4.58; 4.60]	A	< 1	1.2	1.3	2.1	$1.3e^{-2}$	Lin	RH	> 45°

[a]For each date given in column (a), the region extension where rising tones are observed is given in MLT (col. (b), in hours), magnetic latitude (col. (c), in degrees) and in distance to Earth (col. (d), in R_E). In columns (e) and (f), we focus only on the most intense rising tone for each event: the direction of the Poynting flux (col. (e)—A for away, ? for unclear), PSD (col. (f), in nT^2 Hz^{-1}), local He^+ gyrofrequency (col. (g), in Hz), start and maximum frequencies of the rising tone (col. (h) and (i), in Hz), frequency sweep rate (col. (j), in Hz s^{-1}), dominant polarization (col. (k), Lin for linear and Circ for Circular), dominant sense of polarization (col.(l), RH for right-hand and LH for Left hand) and the propagation angle (col. (m), in degrees).

their identification is more complicated. The low latitude of the observations and the quick change of polarization during propagation suggest that the observed EMIC triggered emissions hardly propagate to higher latitudes or to the ground.

[38] The frequency-time shapes of the rising tones happen to be very different when the SC are separated by 240 km (the second event), and they happen to be very similar for larger separations (the third event). There is a need for a dedicated multi-spacecraft analysis to estimate the wavelength and the size of the source region of these triggered emissions.

5. Conclusion

[39] Following the results of *Pickett et al.* [2010], we present new cases of EMIC triggered emissions in the Cluster data. After a systematic STAFF-SC instrument data overview, large triggered emissions are detected in three more Cluster orbits. Orbital properties of the Cluster mission affect the detection in the potential source region of triggered emissions. Further studies need to use data from a spacecraft, which can investigate the range $f_{He^+}/4$–f_{H^+} in the plasmapause region and in the dayside magnetosphere at large L values.

[40] The frequency-time dispersion and the high coherence level are the two main criteria to identify EMIC triggered emissions. Coherence can be used in the future for automated detection [*Lefeuvre and Parrot*, 1979]. The generation occurs in the equatorial region of the magnetosphere as is confirmed by the Poynting flux orientation and by the polarization evolution with the magnetic latitude (from left-hand to linear and even right-hand). The triggering process is generally observed during periods of large AE index values. The four cases are reported between 2001 and 2004 in a period of large solar activity. Short and weak triggered emissions are largely superior in numbers to the large rising tones. Our observations confirm the repetitive nature of the triggering process, which has been reproduced by simulations [*Shoji and Omura*, 2011]. Furthermore, we report the first triggered emission along the He^+ branch. The corresponding event requires further studies to compare the observed properties with recent simulation results [*Shoji and Omura*, 2012] and to establish the sense of propagation and the direction of the Poynting flux. The detailed interactions of the triggered emissions with the particles and the properties of the small and weak rising tones are left for further studies.

References

Anderson, B. J., R. E. Erlandson, and L. J. Zanetti (1992), A statistical study of Pc 1–2 magnetic pulsations in the equatorial magnetosphere. I - Equatorial occurrence distributions. II - Wave properties, *J. Geophys. Res.*, *97*, 3075–3101, doi: 10.1029/91JA02706.

Anderson, H. M., M. J. Engebretson, R. L. Arnoldy, L. J. Cahill, Jr., and P. T. Newell (1995), Statistical study of hydromagnetic chorus events at very high latitudes, *J. Geophys. Res.*, *100*, 3681–3692, doi: 10.1029/94JA02151.

Bossen, M., R. L. McPherron, and C. T. Russell (1976), A statistical study of Pc 1 magnetic pulsations at synchronous orbit, *J. Geophys. Res.*, *81*, 6083–6091, doi: 10.1029/JA081i034p06083.

Clausen, L. B. N., J. B. H. Baker, J. M. Ruohoniemi, and H. J. Singer (2011), EMIC waves observed at geosynchronous orbit during solar minimum: Statistics and excitation, *J. Geophys. Res.*, *116*, A10205, doi: 10.1029/2011JA016823.

Cornilleau-Wehrlin, N., et al. (2003), First results obtained by the Cluster STAFF experiment, *Ann. Geophys.*, *21*, 437–456, doi:10.5194/angeo-21-437-2003.

Cornwall, J. M. (1965), Cyclotron instabilities and electromagnetic emission in the ultra low frequency and very low frequency ranges, *J. Geophys. Res.*, *70*, 61–69, doi: 10.1029/JZ070i001p00061.

Davis, T. N., and M. Sugiura (1966), Auroral electrojet activity index AE and its universal time variations, *J. Geophys. Res.*, *71*(3), 785–801, doi: 10.1029/JZ071i003p00785.

Erlandson, R. E., B. J. Anderson, and L. J. Zanetti (1992), Viking magnetic and electric field observations of periodic Pc 1 waves: Pearl pulsations, *J. Geophys. Res.*, *97*(14), 823, doi: 10.1029/92JA00838.

Escoubet, C., R. Schmidt, and M. Goldstein (1997), Cluster: Science and mission overview, *Space Sci. Rev.*, *79*, 11–32

Fraser, B. J. (1982), Pc 1–2 observations of heavy ion effects by synchronous satellite ATS-6, *Planet. Space Sci.*, *30*, 1229–1238, doi: 10.1016/0032-0633(82)90096-4.

Fukunishi, H., T. Toya, K. Koike, M. Kuwashima, and M. Kawamura (1981), Classification of hydromagnetic emissions based on frequency-time spectra, *J. Geophys. Res.*, *86*, 9029–9039, doi: 10.1029/JA086iA11p09029.

Harang, L. (1936), Oscillations and vibrations in magnetic records at high-latitude stations, *Terr. Magn. Atmos. Elec.*, *41*(4), 329–336, doi: 10.1029/TE041i004p00329.

Helliwell, R. A. (1966), Whistlers and related ionospheric phenomena, *Geophysical Journal International*, *11*, 563–564, doi: 10.1111/j.1365-246X.1966.tb03172.x.

Iyemori, T., K. T., T. Araki, and M. Takeda (1999), *Mid-latitude geomagnetic indices "ASY" and "SYM" for 1999 (Provisional)*. Available at http://swdcwww.kugi.kyoto-u.ac.jp/aeasy/asy.pdf.

Jacobs, J. A., Y. Kato, S. Matsushita, and V. A. Troitskaya (1964), Classification of geomagnetic micropulsations, *J. Geophys. Res.*, *69*, 180–181, doi: 10.1029/JZ069i001p00180.

Kennel, C. F., and H. E. Petschek (1966), Limit on stably trapped particle fluxes, *J. Geophys. Res.*, *71*, 1–28

Labelle, J., R. A. Treumann, W. Baumjohann, G. Haerendel, and N. Sckopke (1988), The duskside plasmapause/ring current interface: Convection and plasma wave observations, *J. Geophys. Res.*, *93*, 2573–2590, doi: 10.1029/JA093iA04p02573.

Lefeuvre, F., and M. Parrot (1979), The use of the coherence function for the automatic recognition of chorus and hiss observed by GEOS, *J. Atmos. Terr. Phy.*, *41*, 143–152

Masson, A., A. Pedersen, M. G. Taylor, C. P. Escoubet, and H. E. Laakso (2009), *Electron density estimation in cold magnetospheric plasmas with the Cluster active archive*. AGU Fall Meeting Abstracts, pp. B1572+.

Mauk, B. H., C. E. McIlwain, and R. L. McPherron (1981), Helium cyclotron resonance within the Earth's magnetosphere, *Geophys. Res. Lett.*, *8*, 103–106, doi: 10.1029/GL008i001p00103.

Moullard, O., A. Masson, H. Laakso, M. Parrot, P. Décréau, O. Santolik, and M. Andre (2002), Density modulated whistler mode emissions observed near the plasmapause, *Geophys. Res. Lett.*, *29*(20), 1975, doi: 10.1029/2002GL015101.

Mursula, K. (2007), Satellite observations of Pc 1 pearl waves: The changing paradigm, *J. Atmos. Sol.-Terr. Phy.*, *69*, 1623–1634, doi: 10.1016/j.jastp.2007.02.013.

Mursula, K., L. G. Blomberg, P.-A. Lindqvist, G. T. Marklund, T. Bräysy, R. Rasinkangas, and P. Tanskanen (1994), Dispersive Pc 1 bursts observed by Freja, *Geophys. Res. Lett.*, *21*, 1851–1854, doi: 10.1029/94GL01584.

Nykyri, K., B. Grison, P. J. Cargill, B. Lavraud, E. Lucek, I. Dandouras, A. Balogh, N. Cornilleau-Wehrlin, and H. Rème (2006), Origin of the turbulent spectra in the high-altitude cusp: Cluster spacecraft observations, *Ann. Geophys.*, *24*, 1057–1075, doi: 10.5194/angeo-24-1057-2006.

Omura, Y., J. Pickett, B. Grison, O. Santolik, I. Dandouras, M. Engebretson, P. M. E. Décréau, and A. Masson (2010), Theory and observation of electromagnetic ion cyclotron triggered emissions in the magnetosphere, *J. Geophys. Res.*, *115* (A07), 234, doi: 10.1029/2010JA015300.

Perraut, S. (1982), Wave-particle interactions in the ULF range: GEOS-1 and -2 results, *Planet. Space Sci.*, *30*, 1219–1227, doi: 10.1016/0032-0633(82)90095-2.

Pickett, J. S., et al. (2010), Cluster observations of EMIC triggered emissions in association with Pc 1 waves near Earth's plasmapause, *Geophys. Res. Lett.*, *37*, 9104–+, doi: 10.1029/2010GL042648.

Roux, A., S. Perraut, J. L. Rauch, C. de Villedary, G. Kremser, A. Korth, and D. T. Young (1982), Wave-particle interactions near Ω_{He^+} observed on board GEOS 1 and 2. II - Generation of ion cyclotron waves and heating of He^+ ions, *J. Geophys. Res.*, *87*, 8174–8190, doi: 10.1029/JA087iA10p08174.

Santolík, O., and D. A. Gurnett (2002), Propagation of auroral hiss at high altitudes, *Geophys. Res. Lett.*, *29* (10), 1481, doi: 10.1029/2001GL013666.

Santolík, O., F. Lefeuvre, M. Parrot, and J. L. Rauch (2001), Complete wave-vector directions of electromagnetic emissions: Application to INTERBALL-2 measurements in the nightside auroral zone, *J. Geophys. Res.*, *106*, 13,191–13,202, doi: 10.1029/2000JA000275.

Santolík, O., J. S. Pickett, D. A. Gurnett, and L. R. O. Storey (2002), Magnetic component of narrowband ion cyclotron waves in the auroral zone, *J. Geophys. Res.*, *107*, 1444, doi: 10.1029/2001JA000146.

Santolík, O., M. Parrot, and F. Lefeuvre (2003), Singular value decomposition methods for wave propagation analysis, *Radio Sci.*, *38*(1), doi: 10.1029/2000RS002523.

Shoji, M., and Y. Omura (2011), Simulation of electromagnetic ion cyclotron triggered emissions in the Earth's inner magnetosphere, *J. Geophys. Res.*, *116*, A05212, doi: 10.1029/2010JA016351.

Shoji, M., and Y. Omura (2012), Precipitation of highly energetic protons by helium branch electromagnetic ion cyclotron triggered emissions, *J. Geophys. Res.*, *117*, A12210, doi: 10.1029/2012JA017933.

Shoji, M., Y. Omura, B. Grison, J. Pickett, I. Dandouras, and M. Engebretson (2011), Electromagnetic ion cyclotron waves in the helium branch induced by multiple electromagnetic ion cyclotron triggered emissions, *Geophys. Res. Lett.*, *38*, L17102, doi:10.1029/2011GL048427.

Sucksdorff, E. (1936), Occurrence of rapid micropulsations at Sodankyla during 1932 to 1935, *Terr. Magn. Atmos. Elec.*, *41*(4), 337–344, doi: 10.1029/TE041i004p00005.

Sugiura, M., and D. Poros, (1971), Hourly values of equatorial DST for years 1957 to 1970, *Tech. Rep. X-645-71-278*, Goddard Space Flight Center, Greenbelt, Maryland.

Troitskaya, V. A. (1961), Pulsation of the Earth's electromagnetic field with periods of 1 to 5 seconds and their connection with phenomena in the high atmosphere, *J. Geophys. Res.*, *66*, 5–18, doi: 10.1029/JZ066i001p00005.

Usanova, M. E., I. R. Mann, J. Bortnik, L. Shao, and V. Angelopoulos (2012), THEMIS Observations of EMIC Wave Occurrence: Dependence on AE, SYMH, and solar wind dynamic pressure, *J. Geophys. Res.*, *117*, A10218, doi: 10.1029/2012JA018049.

Young, D. T., S. Perraut, A. Roux, C. de Villedary, R. Gendrin, A. Korth, G. Kremser, and D. Jones (1981), Wave-particle interactions near Ω_{He^+} observed on GEOS 1 and 2. I - Propagation of ion cyclotron waves in He^+ rich plasma, *J. Geophys. Res.*, *86*, 6755–6772, doi: 10.1029/JA086iA08p06755.